universe

IMPACT FACTOR 2.6

CITESCORE 5.2

Article

Testing Running Vacuum Energy in $f(Q)$ Gravity with DESI Data

Dalale Mhamdi, Redouane El Ouardi, Ahmed Errahmani and Amine Bouali

MDPI

https://doi.org/10.3390/universe12010025

universe

MDPI

Article

Testing Running Vacuum Energy in $f(Q)$ Gravity with DESI Data

Dalale Mhamdi [1,*], Redouane El Ouardi [1], Ahmed Errahmani [1] and Amine Bouali [1,2]

[1] Laboratory of Physics of Matter and Radiations, Mohammed I University, Oujda BP 717, Morocco; redouane.elouardi.d23@ump.ac.ma (R.E.O.); a.errahmani@ump.ac.ma (A.E.); a1.bouali@ump.ac.ma (A.B.)
[2] Higher School of Education and Training, Mohammed I University, Oujda BP 717, Morocco
* Correspondence: dalale.mhamdi@ump.ac.ma

Abstract

In this paper, we investigate the running vacuum energy (RVE) model within the framework of $f(Q)$ gravity ($f(Q)$-RVE). In this context, the modified Friedmann equation can be used to establish a formal analogy with the structure of the RVE. A key feature is that the vacuum equation of state is no longer fixed but receives a dynamical correction proportional to $\dot{H}$ and $\ddot{H}/H$. We consider two cases of $f(Q)$-RVE, denoted as Model I (parametrized by ν) and Model II (parametrized by ν and α), corresponding to the first and second derivatives of H, respectively. The models are constrained using recent DESI BAO data in combination with Pantheon$^+$, cosmic chronometer (CC), and CMB observations. Our analysis shows a deviation of ν from zero at a significance level of $\sim 1.4\sigma$ for Model I, while in Model II, ν and α deviate from zero at 0.7σ and 1.3σ, respectively, relative to ΛCDM. Furthermore, the statistical comparison based on the Akaike, Bayesian, and Deviance Information Criteria (AIC, BIC, DIC) indicates that Model I remains competitive with ΛCDM, while Model II is penalized due to its higher complexity and the sensitivity associated with the additional parameter α.

Keywords: f(Q) gravity; RVE; RVM; DESI; MCMC

1. Introduction

One of the most significant cosmological discoveries is that our Universe is undergoing a phase of late-time accelerated expansion. To explain this phenomenon, scientists have proposed the existence of an exotic form of energy with negative pressure, known as dark energy [1], within the framework of General Relativity (GR). The standard model of cosmology, commonly referred to as the ΛCDM model (Lambda Cold Dark Matter), is the simplest and most widely accepted candidate for describing dark energy, incorporating it as a cosmological constant, denoted by Λ, characterized by an equation of state (EoS) parameter equal to -1, which corresponds to vacuum energy. This cosmological constant acts as a repulsive component in Einstein's field equations, counteracting the attractive nature of gravity and driving the accelerated expansion of the Universe. Although the ΛCDM model fits current cosmological data extremely well, it still faces several challenges, such as the fine-tuning [2,3] and coincidence [4,5] problems. These considerations have led to the proposal of numerous alternatives to the cosmological constant. Among them are effective scalar field models such as quintessence [6–8], phantom [9–13], k-essence [14,15], holographic dark energy [16–21], relativistic fluid models like the Chaplygin gas [22], and dynamical approaches such as running vacuum energy [23–25].

On the other hand, new gravitational theories beyond General Relativity have been proposed to address the challenge of explaining the Universe's accelerated expansion. In

Academic Editor: Pedro Pina Avelino

Received: 31 October 2025
Revised: 6 January 2026
Accepted: 13 January 2026
Published: 15 January 2026

this context, several modified gravity theories have been developed. For instance, $f(R)$ gravity extends General Relativity by replacing the Ricci scalar R in the Einstein-Hilbert action with a general function $f(R)$ [26–28]. This extension aims to account for cosmic acceleration without invoking dark energy. Another class of modifications is based on torsion, $\mathcal{T}$, leading to the so-called teleparallel formulation of gravity, which serves as the foundation for extended theories such as $f(\mathcal{T})$ gravity [29–32]. In this framework, torsion rather than curvature governs the gravitational interaction. Besides these aforementioned modified gravity theories, symmetric teleparallel gravity provides an alternative approach by relying on the non-metricity scalar, Q, to describe gravitational effects. This theory belongs to the metric-affine geometry, where gravity is characterized by variations in vector lengths rather than their directions, distinguishing it from other geometric formulations [33–43]. Additionally, another class of modified gravity theories emerges from the inclusion of the trace of the energy–momentum tensor of matter, T, leading to extensions such as $f(R,T)$ gravity [44–46] and $f(Q,T)$ gravity [47–49]. Among these, $f(Q)$ gravity has recently attracted growing interest due to its theoretical simplicity, second-order field equations, and its ability to explore gravitational phenomena in both the early and late Universe through a distinctive geometrical framework grounded in non-metricity.

Moreover, within the framework of General Relativity, a dynamical vacuum energy density can naturally arise from quantum effects computed in Quantum Field Theory (QFT) formulated on curved space-time backgrounds [50,51]. In this context, the vacuum energy density is typically expressed as a series expansion involving even powers of the Hubble parameter, H, and, in some formulations, its derivatives with respect to cosmic time. This dynamical vacuum structure is commonly referred to as the Running Vacuum Energy(RVE) model [23–25], which has garnered considerable interest in recent years due to its potential to unify early and late-time cosmic acceleration. Specifically, the RVE framework has been proposed to account for both the inflationary phase in the early Universe, referred to as RVM-inflation [52–55], and the observed acceleration at late times [56,57]. At late times, the running of the vacuum energy density is typically modeled as a function of H and its first derivative $\dot{H}$ [23,24,58], consistent with general covariance and QFT expectations. Recent studies [24,59,60] have demonstrated that the effective equation of state of the vacuum energy in this framework is generally not constant and can deviate from the exact cosmological constant value $\omega = -1$, evolving dynamically with the expansion history of the Universe.

Furthermore, the Running Vacuum Model (RVE) postulates that the vacuum energy density $\rho_{\rm vac}$ evolves with cosmic time as a consequence of quantum effects associated with matter fields [61]. These effects can be formally described using the renormalization group equation applied to the effective action [55], leading to a dynamical expression for $\rho_{\rm vac}$ in terms of the Hubble parameter H and its time derivatives. In parallel, the symmetric teleparallel formulation of gravity, described within the $f(Q)$ framework, provides a geometrically consistent theoretical framework in which a similar dynamical behavior may naturally emerge. In a spatially flat FLRW Universe, the modified Friedmann equations include specific combinations such as $F_Q + 2QF_{QQ}$ and $(F/2 - QF_Q)$, which can be expressed in terms of quantities like H^2, $\dot{H}/H^2$, and $\ddot{H}/(H\dot{H})$, establishing a formal analogy with the structure of the RVE. This correspondence motivates our investigation of the running vacuum paradigm within the context of $f(Q)$ gravity. We explore two dynamical scenarios in which the quantity $F_Q + 2QF_{QQ}$ adopts distinct functional forms. In the first case, it is taken to be constant, while in the second, it includes an additional correction term containing the term $\ddot{H}/(H\dot{H})$. These assumptions lead to two different expressions for the vacuum energy density, and in each case, we derive the corresponding modified Friedmann equations.

https://doi.org/10.3390/universe12010025

To constrain cosmological parameters associated with the two proposed scenarios, we perform a Markov Chain Monte Carlo (MCMC) analysis [62], using a combination of recent observational datasets. These include cosmic chronometer $H(z)$ measurements, the Pantheon$^+$ compilation of Type Ia supernovae, Baryon Acoustic Oscillations (BAO) data, including the latest results from the Dark Energy Spectroscopic Instrument (DESI), and Cosmic Microwave Background (CMB) observations. Subsequently, we compare the performance of our models with the standard ΛCDM scenario using statistical model selection criteria, namely the Akaike Information Criterion (AIC) [63,64], the Bayesian Information Criterion (BIC) [65], and the Deviance Information Criterion (DIC) [66].

The structure of this paper is as follows. In Section 2, we provide a brief introduction to $f(Q)$ gravity. In Section 3, we present the modified Friedmann equations derived within this framework and introduce the dynamical scenarios under consideration. Section 4 outlines the methodology used to constrain the model parameters, including a description of the Markov Chain Monte Carlo (MCMC) approach, the observational datasets used in the analysis, and the statistical techniques adopted for model selection and comparison. In Section 5, we report the mean values of the cosmological parameters and present the results of the model selection criteria. Finally, in Section 6, we summarize our main findings and highlight the key conclusions of the work. Throughout this paper, we adopt natural units by setting $G = c = 1$, and we define the gravitational constant as $\kappa^2 = 8\pi G$.

2. Overview of $f(Q)$ Gravity

In this section, we give a brief introduction to the formalism of $f(Q)$ gravity. We consider a $f(Q)$ modified gravity, in which the basic object is the non-metricity tensor, $Q_{\lambda\mu\nu}$, given by [33]

$$\Delta_\lambda g_{\mu\nu} = Q_{\lambda\mu\nu}. \tag{1}$$

The non-metricity scalar is defined as follows

$$Q = -g^{\mu\nu}(L^\alpha_{\beta\nu}L^\beta_{\nu\alpha} - L^\alpha_{\beta\alpha}L^\beta_{\mu\nu}), \tag{2}$$

with $L^\lambda_{\mu\nu}$ is the disformation tensor symmetrical with respect to lower indices given by

$$L^\lambda_{\mu\nu} = -\frac{1}{2}g^{\lambda\gamma}(Q_{\mu\gamma\nu} + Q_{\nu\gamma\mu} - Q_{\gamma\mu\nu}). \tag{3}$$

The $f(Q)$ gravity action is written as follows [39]

$$S = \int \sqrt{-g}d^4x\left[\frac{1}{2\kappa^2}f(Q) + \mathcal{L}_m\right], \tag{4}$$

where $f(Q)$ is a function of the non-metricity scalar, g is the determinant of the metric $g_{\mu\nu}$ and $\mathcal{L}_m$ is the Lagrangian density of matter. The non-metricity tensor, Equation (1), can be rewritten as

$$Q_{\alpha\mu\nu} = \Delta_\alpha g_{\mu\nu} = -L^\rho_{\alpha\mu}g_{\rho\nu} - L^\rho_{\alpha\nu}g_{\rho\mu}. \tag{5}$$

The following equations give the expressions of the two independent traces of the non-metricity tensor,

$$Q_\alpha = Q_\alpha{}^\beta{}_\beta\,, \qquad \tilde{Q}^\alpha = Q_\beta{}^{\alpha\beta}, \tag{6}$$

while the disformation term is given by

$$L^\alpha{}_{\mu\nu} = \frac{1}{2}Q^\alpha{}_{\mu\nu} - Q_{(\mu}{}^\alpha{}_{\nu)}. \tag{7}$$

Moreover, the non-metricity scalar, Q, Equation (2) becomes

$$Q = -g^{\mu\nu}(L^{\alpha}_{\beta\nu}L^{\beta}_{\mu\alpha} - L^{\beta}_{\alpha\beta}L^{\alpha}_{\mu\nu}) = -P^{\alpha\beta\gamma}Q_{\alpha\beta\gamma}, \tag{8}$$

where $P^{\alpha\beta\gamma}$ is the non-metricity conjugate, defined as

$$P^{\alpha}_{\mu\nu} = -\frac{1}{2}L^{\alpha}_{\mu\nu} + \frac{1}{4}(Q^{\alpha} - \tilde{Q}^{\alpha})g_{\mu\nu} - \frac{1}{4}\delta^{\alpha}_{(\mu}Q_{\nu)}. \tag{9}$$

The field equation of the $f(Q)$ gravity is obtained by varying the action (4) with respect to the metric, and it takes the following form

$$\frac{-2}{\sqrt{-g}}\nabla_{\alpha}\left(\sqrt{-g}f_{Q}P^{\alpha}_{\mu\nu}\right) - \frac{1}{2}g_{\mu\nu}f - f_{Q}\left(P_{\mu\alpha\beta}Q_{\nu}{}^{\alpha\beta} - 2Q_{\alpha\beta\mu}P^{\alpha\beta}_{\nu}\right) = \kappa T_{\mu\nu} \tag{10}$$

and the energy–momentum tensor, $T_{\mu\nu}$ is given by

$$T_{\mu\nu} = -\frac{2}{\sqrt{-g}}\frac{\delta(\sqrt{-g}\mathcal{L}_{m})}{\delta\sqrt{g_{\mu\nu}}}, \tag{11}$$

Furthermore, by varying the action (4) with respect to the affine connection [39], we obtain the following equation

$$\nabla_{\mu}\nabla_{\nu}(\sqrt{-g}f_{Q}P^{\mu\nu}_{\alpha}) = 0. \tag{12}$$

3. Cosmological Model

The standard Friedmann–Lemaître–Robertson–Walker (FLRW) line element, which describes the flat, homogeneous, and isotropic Universe, is given by

$$ds^2 = -dt^2 + a^2(t)\left(dx^2 + dy^2 + dz^2\right), \tag{13}$$

where t is the cosmic time, x, y and z denote the Cartesian coordinates, $a(t)$ is the cosmic scale factor, and the Hubble parameter $H(t)$ is defined by $H(t) = \frac{\dot{a}}{a}$, with $\dot{a}$ denotes the derivative of a with respect to the cosmic time, t. Moreover, the cosmological redshift z is defined as $1 + z = 1/a$.

3.1. The Generalized Friedmann Equations

In the FLRW geometry, we obtain the non-metricity scalar as $Q = 6H^2$. We consider the matter content of the Universe as consisting of a perfect and isotropic fluid, with energy–momentum tensor given by

$$T_{\mu\nu} = (p + \rho)u_{\mu}u_{\nu} + pg_{\mu\nu}, \tag{14}$$

where p and ρ are the pressure and the energy density of the fluid, respectively, u_{μ} is the four velocity vector normalized according to $u^{\mu}u_{\nu} = -1$.

We now consider the splitting of $f(Q)$ as $f(Q) = Q + F(Q)$. Using the FLRW metric, we obtain two Friedmann equations as

$$\begin{cases} -\dfrac{F}{2} + 3H^2 + QF_{Q} = \kappa^2\rho, \\ \left(12F_{QQ}H^2 + 1 + F_{Q}\right)\dot{H} = -\dfrac{\kappa^2}{2}(\rho + p). \end{cases} \tag{15}$$

According to Equation (15), we return to the standard model, for $F = 0$ (i.e., $f(Q) = Q$). The same equation gives

$$\begin{cases} \kappa^2\rho = 3H^2 - \frac{F}{2} + QF_Q, \\ \kappa^2 p = -2\dot{H} - 3H^2 - 2\dot{H}(F_Q + 2QF_{QQ}) \\ \qquad\qquad + \frac{1}{2}F - QF_Q. \end{cases} \tag{16}$$

with

$$\begin{cases} 3H^2 = \kappa^2(\rho + \rho_{DE}), \\ -2\dot{H} - 3H^2 = \kappa^2(p + p_{DE}). \end{cases} \tag{17}$$

Using Equations (16) and (17), we obtain the dark energy density and its pressure, respectively, as follows

$$\begin{cases} \kappa^2\rho_{DE} = \frac{F}{2} - QF_Q, \\ \kappa^2 p_{DE} = 2\dot{H}(F_Q + 2QF_{QQ}) - \frac{F}{2} + QF_Q, \end{cases} \tag{18}$$

which give

$$\kappa^2(p_{DE} + \rho_{DE}) = 2\dot{H}(F_Q + 2QF_{QQ}). \tag{19}$$

Equation (19) reduces to $p_{DE} = -\rho_{DE}$ in the case where $F_Q + 2QF_{QQ} = 0$, i.e., $\frac{d}{dQ}(\frac{F}{2} - QF_Q) = 0$, which represents the derivative of ρ_{DE} with respect to Q. This case corresponds to the cosmological constant, i.e., to $f(Q) = Q + c_1\sqrt{Q} + c_2$, where c_1 and c_2 are constants.

In general cases, we can take $F_Q + 2QF_{QQ} \neq 0$. Furthermore, one can see from Equation (19) that $F_Q + 2QF_{QQ}$ has no dimension, and subsequently, this term can be assumed to depend on dimensionless combinations such as $\frac{\dot{H}}{H^2}$ or $\frac{\ddot{H}}{H\dot{H}}$, etc. The same remark regarding the term $\frac{F}{2} - QF_Q$ in Equation (18), which has the dimension of H^2 can be expressed as H^2, $\dot{H}$, $\frac{\ddot{H}}{\dot{H}}$, etc.

3.2. Running Vacuum Energy in $f(Q)$ Gravity

In the context of quantum field theory in curved spacetime, explicit calculations of quantum effects lead to the Running Vacuum energy density, ρ_{vac}, as [50,52,67,68]

$$\rho_{vac}(H) = \frac{3}{\kappa^2}(c_0 + \nu H^2 + \frac{2}{3}\alpha\dot{H} + \mu\frac{H^4}{H_I} + \dots). \tag{20}$$

The dots represent higher-order powers of H, and c_0 is a positive constant related to the cosmological constant. The coefficients ν, α, and μ are relatively small because they control the dynamics of the vacuum energy density. The parameter H_I represents the Hubble scale during the inflationary epoch. It should be stressed that the H^4 term is relevant exclusively in the very early Universe. Such a contribution can induce an inflationary phase through a mechanism different from other inflationary models, including Starobinsky inflation (see the detailed analysis in [69]), in which the origin of these terms is fully established and not treated as a mere assumption. However, as we are examining the present Universe, the H^4 term will be neglected by setting $\mu = 0$ for our study. The most general realization of the running vacuum framework describing the present Universe, and analyzed extensively in the literature, is given by [50,59,70,71]

$$\rho_{vac}(H) = \frac{3}{\kappa^2}(c_0 + \nu H^2 + \frac{2}{3}\alpha\dot{H}). \tag{21}$$

The equation of state for the Running Vacuum Models (RVE) resembles that of an ideal de Sitter fluid, despite the time-varying nature of the vacuum energy. Consequently,

$$p_{vac}(H) = -\rho_{vac}(H), \tag{22}$$

where $p_{vac}(H)$ denotes the vacuum pressure density.

Recent studies, conducted by the authors of [23,50–52,68], have calculated the equation of state for the running vacuum energy within the framework of quantum field theory. They have shown that this equation of state is not exactly equal to -1 but becomes dynamical and influenced by various factors associated with cosmic expansion, i.e., the running vacuum energy evolves as a function of the Hubble parameter and its derivatives, $\omega = \omega(H, \dot{H}, \ddot{H}, \dots)$. In the first order

$$p_{vac}(H) + \rho_{vac}(H) = -\frac{\nu}{\kappa^2}\dot{H} \tag{23}$$

In the following of this work, we consider dark energy as a running vacuum model and will discuss two cases by limiting ourselves to the first and second orders of Equation (19) in terms of $H, \dot{H}, \ddot{H}$, etc.

3.2.1. Model I: $F_Q + 2QF_{QQ} = cte$

A straightforward case for $p_{DE} + \rho_{DE} \neq 0$ is to assume:

$$F_Q + 2QF_{QQ} = -\nu, \tag{24}$$

where ν is a constant. This case corresponds to $f(Q) = (1-\nu)Q + k_1\sqrt{Q} + k_2$ where k_1 and k_2 are constants. The equation of state, Equation (19), then becomes

$$p_{\rm vac}(H) + \rho_{\rm vac}(H) = -2\frac{\nu}{\kappa^2}\dot{H}. \tag{25}$$

The integration of Equation (24) yields

$$\rho_{vac} = \frac{1}{\kappa^2}\left(\frac{F}{2} - QF_Q\right) = \frac{3}{\kappa^2}(c_0 + \nu H^2). \tag{26}$$

Comparing the last two equations to Equations (18) and (23), we conclude that our model is equivalent to RVE at first order.

We assume that the cosmic fluid consists of radiation, cold dark matter and running vacuum energy, the Friedmann Equation (17) can be rewritten as

$$3H^2 = \kappa^2\rho_{m0}(1+z)^3 + \kappa^2\rho_{r0}(1+z)^4 + 3(c_0 + \nu H^2). \tag{27}$$

At $z = 0$, the constant is given by $c_0 = (1 - \nu - \Omega_{m0} - \Omega_{r0})H_0^2$, and the corresponding normalized Hubble parameter, denoted as $E = H/H_0$, can be expressed as

$$E^2 = 1 + \frac{\Omega_{m0}}{1-\nu}\left[(1+z)^3 - 1\right] + \frac{\Omega_{r0}}{1-\nu}\left[(1+z)^4 - 1\right], \tag{28}$$

where Ω_{m0} and Ω_{r0} represent the actual matter and radiation densities, respectively.

3.2.2. Model II: $F_Q + 2QF_{QQ} = -(\nu + \frac{\alpha}{3}\frac{\ddot{H}}{H\dot{H}})$

For the second order, we can write the term $F_Q + 2QF_{QQ}$ as follows

$$F_Q + 2QF_{QQ} = -\left(\nu + \frac{\alpha}{3}\frac{\ddot{H}}{H\dot{H}}\right) \tag{29}$$

where ν and α are constants. In this scenario, the analytical expression of $f(Q)$ cannot be obtained explicitly. The equation of state in this case can be written as

$$p_{vac}(H) + \rho_{vac}(H) = -\frac{2}{\kappa^2}(\nu\dot{H} + \frac{\alpha}{3}\frac{\ddot{H}}{H}). \tag{30}$$

The integration of Equation (29) yields

$$\rho_{vac}(H) = \frac{3}{\kappa^2}(c_0 + \nu H^2 + \frac{2}{3}\alpha\dot{H}). \tag{31}$$

This equation is the same as Equation (21) which mean that $f(Q)$ gravity is equivalent to RVE in second order. The Friedmann equation in this case can be written as

$$3H^2 = \kappa^2\rho_{m0}(1+z)^3 + \kappa^2\rho_{r0}(1+z)^4 + 3(c_0 + \nu H^2 + \frac{2}{3}\alpha\dot{H}) \tag{32}$$

$$\frac{\alpha}{3}\frac{dE^2}{dz}(1+z) + (1-\nu)E^2 = \Omega_{m0}(1+z)^3 + \Omega_{r0}(1+z)^4 + \frac{c_0}{H_0^2}. \tag{33}$$

The analytical solution to this differential equation is

$$\begin{aligned} E^2 = {} & \frac{\Omega_{m0}}{1+\alpha-\nu}(1+z)^3 + \frac{3\Omega_{r0}}{3+4\alpha-3\nu}(1+z)^4 \\ & + c_1(1+z)^{-3\frac{(1-\nu)}{\alpha}} + \frac{c_0}{(1-\nu)H_0^2} \end{aligned} \tag{34}$$

with

$$c_1 = 1 - \frac{\Omega_{m0}}{1+\alpha-\nu} - \frac{3\Omega_{r0}}{3+4\alpha-3\nu} - \frac{c_0}{(1-\nu)H_0^2} \tag{35}$$

4. Observational Datasets and Methodology

In this section, we present the observational datasets and the statistical methodology employed to constrain the Running Vacuum Energy models considered in this work. The primary dataset used is the recent DESI survey, which includes samples of bright galaxies (BGS), luminous red galaxies (LRGs), emission line galaxies (ELGs), quasars, and the Lyα forest over the redshift range $0.1 \leq z \leq 2.33$ [72]. From this dataset, we use the measurements of the comoving distances $D_M(z)/r_d$ and $D_H(z)/r_d$, defined as

$$D_M(z) \equiv \int_0^z \frac{c\,dz'}{H(z')}, \quad \text{and} \quad D_H(z) \equiv \frac{c}{H(z)}. \tag{36}$$

For standard early-time physics, the drag-epoch sound horizon is approximated by [73,74]:

$$r_{\rm d} = 147.05\left(\frac{\omega_{\rm m}}{0.1432}\right)^{-0.23}\left(\frac{N_{\rm eff}}{3.04}\right)^{-0.1}\left(\frac{\omega_{\rm b}}{0.02236}\right)^{-0.13}, \tag{37}$$

where $\omega_m = \Omega_m h^2$ and $\omega_b = \Omega_b h^2$ denote the physical matter and baryon density parameters, respectively, and $N_{\rm eff}$ denotes the effective number of relativistic species. In this work, we fix $N_{\rm eff} = 3.044$ [75]. We also consider the angle-averaged distance $D_V(z)/r_d$, given by

$$D_V(z) \equiv \left[z\,D_M(z)^2\,D_H(z)\right]^{1/3}. \tag{38}$$

The BAO distance measurements from the DESI Year-1 data are summarized in Table 1. The dataset comprises 12 data points, of which five (at redshifts $z = 0.51$, 0.71, 0.93, 1.32, and 2.33) are correlated. The corresponding covariance matrices are provided in Table 2.

In this analysis, to investigate the cosmological implications of the RVE-$f(Q)$ models using DESI BAO data, we also include the following complementary datasets

- **Planck 2018 CMB data:** Providing constraints through the acoustic scale l_a, shift parameter R, and baryon density ω_b [75].
- **Pantheon$^+$ SNIa dataset:** Containing 1550 Type Ia supernovae over the redshift range $0.001 \leq z \leq 2.3$ [76].
- **Cosmic Chronometers:** Including 36 $H(z)$ measurements obtained via the differential age method [77].

Table 1. DESI Year-1 BAO distance measurements.

Redshift	Measurement	Type	Tracer
0.295	7.93	D_V/r_d	BGS
0.51	13.62	D_M/r_d	LRG1
0.51	20.98	D_H/r_d	LRG1
0.71	16.85	D_M/r_d	LRG2
0.71	20.08	D_H/r_d	LRG2
0.93	21.71	D_M/r_d	LRG3+ELG1
0.93	17.88	D_H/r_d	LRG3+ELG1
1.32	27.79	D_M/r_d	ELG2
1.32	13.82	D_H/r_d	ELG2
1.49	26.07	D_V/r_d	QSO
2.33	39.71	D_M/r_d	Lyα QSO
2.33	8.52	D_H/r_d	Lyα QSO

Table 2. Covariance matrices $C(z)$ for DESI BAO measurements.

Redshift	$C(z)$
0.51	$\begin{pmatrix} 0.0625 & -0.0679 \\ -0.0679 & 0.3721 \end{pmatrix}$
0.71	$\begin{pmatrix} 0.1024 & -0.0806 \\ -0.0806 & 0.36 \end{pmatrix}$
0.93	$\begin{pmatrix} 0.0784 & -0.0381 \\ -0.0381 & 0.1225 \end{pmatrix}$
1.32	$\begin{pmatrix} 0.4761 & -0.1287 \\ -0.1287 & 0.1764 \end{pmatrix}$
2.33	$\begin{pmatrix} 0.8836 & -0.0762 \\ -0.0762 & 0.0289 \end{pmatrix}$

We now turn to the statistical methodology adopted in this work. To constrain the RVE-$f(Q)$ models, we employ a Markov Chain Monte Carlo technique, which is widely used in cosmology to explore the parameter space of complex models and to derive probability distributions for cosmological parameters [78]. The fundamental idea behind MCMC is to construct a Markov chain that samples the model's parameter space according to a target probability distribution. The chain consists of a sequence of parameter values, where each new value is generated from the preceding one using transition rules defined by a proposal distribution [78,79]. In our analysis, we constrain two RVE-$f(Q)$ models:

- **Model I**: with free parameters $(\Omega_m, h, \omega_b, \nu)$,
- **Model II**: with free parameters $(\Omega_m, h, \omega_b, \nu, \alpha, \beta)$.

Here, h is related to the Hubble constant by $H_0 = 100\,h$, while $\beta = c_0/(3H_0^2)$ is the dimensionless parameter. The free parameters are constrained by minimizing the total chi-squared function, defined as

$$\chi^2_{\rm tot} = \chi^2_{\rm DESI} + \chi^2_{\rm SN} + \chi^2_{CC} + \chi^2_{\rm CMB}, \tag{39}$$

where each term represents the contribution from the corresponding dataset. For uncorrelated data points, χ^2 is given by

$$\chi^2 = \sum_{i=1}^{N} \frac{(D_i - T_i)^2}{\sigma_i^2}, \tag{40}$$

with D_i the observed value, T_i the theoretical prediction, and σ_i the associated uncertainty. In the presence of correlations between data points, the chi-square generalizes to the matrix form

$$\chi^2 = \Delta\mathbf{D}^T \cdot \mathbf{C}^{-1} \cdot \Delta\mathbf{D}, \tag{41}$$

where $\Delta\mathbf{D} = \mathbf{D} - \mathbf{T}$ is the residual vector, and $\mathbf{C}$ is the covariance matrix encoding both statistical and systematic correlations.

By computing the minimum value, $\chi^2_{\rm min}$, we can derive the information criteria used to assess the performance of the models. The corrected Akaike Information Criterion (AIC_c) and the Bayesian Information Criterion (BIC) are given by [64,65]

$$AIC_c = \chi^2_{\rm min} + 2K_f + \frac{2K_f(K_f+1)}{N_t - K_f - 1}, \tag{42}$$

$$\mathrm{BIC} = \chi^2_{\rm min} + K_f \ln(N_t), \tag{43}$$

where K_f denotes the number of free parameters, and N_t is the total number of data points. In addition, we also consider the Deviance Information Criterion (DIC), which combines elements of Bayesian statistics and information theory. It is defined as [66]

$$\mathrm{DIC} = D(\bar{p}) + 2C_B, \tag{44}$$

where C_B is the Bayesian complexity, expressed as $C_B = \overline{D(p)} - D(\bar{p})$, with the overline denoting an average over the posterior distribution. Here, $D(p)$ is the Bayesian deviance, which can be expressed as $D(p) = \chi^2_{\rm tot}(p)$. Among competing models, the one with the lowest values of AIC_c, BIC, and DIC is considered to be the most supported by the observational data and is chosen as the reference model.

5. Results and Discussion

In this section, we present the results of our analysis regarding the two RVE-$f(Q)$ cosmological models. We test two specific cases: Model I and Model II, described by the Friedmann Equations (28) and (34), respectively. The free parameters of these models are constrained using the combined datasets Pantheon$^+$ + CC, DESI BAO + CC, CMB + CC, as well as the joint dataset DESI BAO + Pantheon$^+$ + CC + CMB. Table 3 summarizes the MCMC results for the ΛCDM model and the two RVE-$f(Q)$ models. It lists the prior distributions of the free parameters adopted in the MCMC analysis, together with their mean values and associated 1σ errors, as well as the values of $\chi^2_{\rm min}$, $\chi^2_{d.o.f}$, AIC, BIC, DIC, and their differences ΔIC [1]. The free parameter vector of the ΛCDM model is $\{\Omega_m, h, \omega_b, \mathcal{M}\}$. For Model I, it is $\{\Omega_m, h, \omega_b, \mathcal{M}, \nu\}$, while for Model II it is $\{\Omega_m, h, \omega_b, \mathcal{M}, \nu, \alpha, \beta\}$, where the parameter $\mathcal{M}$ represents the absolute magnitude of Type Ia supernovae.

For the Pantheon$^+$ CC data combination, the ΛCDM model yields $\Omega_m = 0.282 \pm 0.0126$, $h = 0.7143 \pm 0.0084$, and $\mathcal{M} = -19.324 \pm 0.024$. Relative to Model I and Model II of the RVE-$f(Q)$ framework, these values display only mild differences, with all tensions remaining below the 1σ level. In particular, the estimates of h and $\mathcal{M}$ show excellent agreement among the models, while the constraints on Ω_m are statistically consistent within 1σ. When DESI BAO data are combined with CC measurements, we obtain $\Omega_m = 0.2758 \pm 0.0156$, $h = 0.6925 \pm 0.0148$, and $\omega_b = 0.02345 \pm 0.00237$ for the ΛCDM scenario. The corresponding constraints inferred for Model I and Model II remain compatible with these values, with no parameter exhibiting deviations beyond the 1σ level. The parameters Ω_m, h, and ω_b are therefore mutually consistent across all models within this dataset combination. The joint analysis of CMB and CC data leads to $\Omega_m = 0.3045 \pm 0.0088$, $h = 0.6844 \pm 0.0066$, and $\omega_b = 0.02249 \pm 0.00016$ in the context of ΛCDM. While modest shifts in h are observed when compared to the RVE-$f(Q)$ extensions, they remain well within 1σ, and both Ω_m and ω_b show full consistency across the models. Overall, none of the considered dataset combinations reveals statistically significant tension between the ΛCDM and RVE-$f(Q)$ frameworks. By constraining ΛCDM and RVE-$f(Q)$ models with DESI BAO + Pantheon$^+$ + CC + CMB datasets, we find $\Omega_m = 0.293 \pm 0.0051$ for the ΛCDM model. This estimate is about 0.1σ higher than that of Model I, $\Omega_m = 0.2855 \pm 0.0073$, and about 0.7σ lower than that of Model II, $\Omega_m = 0.310 \pm 0.024$. Regarding the Hubble parameter, we obtain $h = 0.6934 \pm 0.004\,\mathrm{km\,s^{-1}Mpc^{-1}}$ for ΛCDM, which is closer to the value of Model I, $h = 0.6964 \pm 0.0046\,\mathrm{km\,s^{-1}Mpc^{-1}}$, with a deviation of about 0.5σ. Both ΛCDM and Model I are significantly different from Model II, $h = 0.665 \pm 0.029\,\mathrm{km\,s^{-1}Mpc^{-1}}$, with tensions of 0.97σ and 1.07σ, respectively. The baryonic parameter ω_b is consistent across the three models, with values around 0.0226. Similarly, the absolute magnitude $\mathcal{M}$ remains nearly identical, with values close to -19.4.

Now, let us turn to the RVE parameters of greatest interest in this work, namely ν, α, and β, as they quantify the deviation of the running vacuum density from the cosmological constant ΛCDM. Concerning Model I, using the Pantheon$^+$ + CC, DESI BAO + CC, and CMB + CC dataset combinations, we find that the parameter ν differs from zero at approximately 6.25σ, 1.67σ, and 2.23σ, respectively, with corresponding values $\nu = -0.0637 \pm 0.0102$, $\nu = -0.1078 \pm 0.0646$, and $\nu = -0.0332 \pm 0.0149$. However, using the combined dataset DESI BAO + Pantheon$^+$ + CC + CMB, we obtain the model parameter $\nu = -0.0133 \pm 0.0094$, which implies that the value of ν differs from zero at approximately 1.4σ (see Figure 1). At this point, it is worth noting that our model exhibits a fundamental distinction from the RVE framework [80]. Specifically, in our formulation no interaction is assumed between the RVE component and the matter–energy density. This contrasts with the RVE model, where an explicit coupling between the cosmological fluid and the RVE sector plays a key role in the dynamical evolution of the Universe. Considering the first-order term νH^2 from Equation (20), the authors in [80] studied a model of running vacuum density with a perfect fluid with an equation of state $\omega_{\mathrm{de}} = -1$, which differs from our case ($\omega_{\mathrm{de}} \neq -1$). Using the dataset SN Ia + CMB + BAO, they obtained $\nu = 0.0048 \pm 0.0018$, finding that the value differs from zero at $\sim 2.7\sigma$. With an extended dataset SN Ia + CMB + BAO + OHD, the significance of a non-zero ν improved considerably to 3.4σ. In another comparison, [81,82] considered a model of running vacuum interacting with dark matter. They performed a joint likelihood analysis using supernovae data from the JLA sample, the CMB power spectrum, BAO, and $H(z)$ measurements. Three models were considered, each with a different choice for the phenomenological interaction term Q. Among these, the model with $Q = \nu H(3\rho_m + 4\rho_r)$ exhibits a small but non-zero deviation from ΛCDM. Specifically, they found that the deviation parameter ν differs from zero at the 2.5σ level.

Table 3. Prior ranges and mean values of the cosmological parameters for the ΛCDM model and the RVE-$f(Q)$ scenarios (Model I and Model II), obtained using different combinations of observational data: Pantheon$^+$ + CC, DESI BAO + CC, CMB + CC, and the full combined dataset DESI BAO + Pantheon$^+$ + CC + CMB. Quoted uncertainties correspond to 1σ confidence levels. The lower panel reports the corresponding statistical model comparison results, including $\chi^2_{\rm min}$, $\chi^2_{\rm d.o.f}$, AIC, BIC, and DIC.

Parameter	Prior Range	ΛCDM	RVE-$f(Q)$	
			Model I	Model II
		Pantheon$^+$ + CC		
Ω_m	$[0,1]$	0.2822 ± 0.0126	0.3000 ± 0.0140	0.3893 ± 0.0438
h	$[0.5,1]$	0.7143 ± 0.0084	0.7143 ± 0.0087	0.7081 ± 0.0130
ν	$[-0.2,0.2]$	–	-0.0637 ± 0.0102	-0.1510 ± 0.0876
β	$[0,1]$	–	–	0.3169 ± 0.0288
α	$[0,1]$	–	–	0.3236 ± 0.1464
$\mathcal{M}$	$[-20,-19]$	-19.324 ± 0.024	-19.324 ± 0.024	-19.308 ± 0.025
$\chi^2_{\rm min}$		1564.16	1564.15	1555.29
		DESI BAO + CC		
Ω_m	$[0,1]$	0.2758 ± 0.0156	0.3056 ± 0.0248	0.3294 ± 0.0433
h	$[0.5,1]$	0.6925 ± 0.0148	0.6924 ± 0.0151	0.6481 ± 0.0513
ω_b	$[0,0.05]$	0.02345 ± 0.00237	0.01975 ± 0.00298	0.0226 ± 0.00242
ν	$[-0.2,0.2]$	–	-0.1078 ± 0.0646	0.0851 ± 0.0786
β	$[0,1]$	–	–	0.2697 ± 0.0460
α	$[0,1]$	–	–	0.1363 ± 0.0842
$\chi^2_{\rm min}$		33.84	33.84	30.95
		CMB + CC		
Ω_m	$[0,1]$	0.3045 ± 0.0088	0.2700 ± 0.0159	0.3159 ± 0.0470
h	$[0.5,1]$	0.6844 ± 0.0066	0.7048 ± 0.0108	0.6486 ± 0.0456
ω_b	$[0,0.05]$	0.02249 ± 0.00016	0.02247 ± 0.00016	0.02249 ± 0.00016
ν	$[-0.2,0.2]$	–	-0.0332 ± 0.0149	0.0431 ± 0.0558
β	$[0,1]$	–	–	0.2779 ± 0.0478
α	$[0,1]$	–	–	0.0755 ± 0.0494
$\chi^2_{\rm min}$		22.92	19.55	19.49
		DESI BAO + Pantheon$^+$ + CC + CMB		
Ω_m	$[0,1]$	0.2930 ± 0.0051	0.2855 ± 0.0073	$0.310^{+0.024}_{-0.031}$
h	$[0.5,1]$	0.6934 ± 0.0040	0.6964 ± 0.0046	$0.665^{+0.029}_{-0.026}$
ω_b	$[0,0.05]$	0.02268 ± 0.00013	0.02258 ± 0.00015	0.02257 ± 0.00014
ν	$[-0.2,0.2]$	–	-0.0133 ± 0.0094	$-0.0073^{+0.011}_{-0.0096}$
β	$[0,1]$	–	–	$0.270^{+0.022}_{-0.027}$
α	$[0,1]$	–	–	$0.0118^{+0.0076}_{-0.011}$
$\mathcal{M}$	$[-20,-19]$	-19.404 ± 0.012	-19.403 ± 0.012	-19.383 ± 0.011
$\chi^2_{\rm min}$		1587.68	1585.62	1584.10
		Statistical Results (Full Dataset)		
$\chi^2_{\rm d.o.f}$		0.9083	0.9076	0.9078
AIC		1595.70	1595.65	1598.16
BIC		1617.55	1622.96	1636.38
DIC		1596.47	1596.31	1596.57
ΔAIC		0	−0.05	2.46
ΔBIC		0	2.46	18.83
ΔDIC		0	−0.16	0.24

The reduced chi-square is defined as $\chi^2_{\rm d.o.f} = \chi^2_{\rm min}/(N_t - K_f)$. The interpretation of ΔIC is as follows: $|\Delta{\rm IC}| \leq 2$ indicates substantial observational support for the fitted data, $2 < |\Delta{\rm IC}| \leq 6$ indicates moderate support, $6 < |\Delta{\rm IC}| \leq 10$ indicates weak support, and $|\Delta{\rm IC}| > 10$ signifies no observational support.

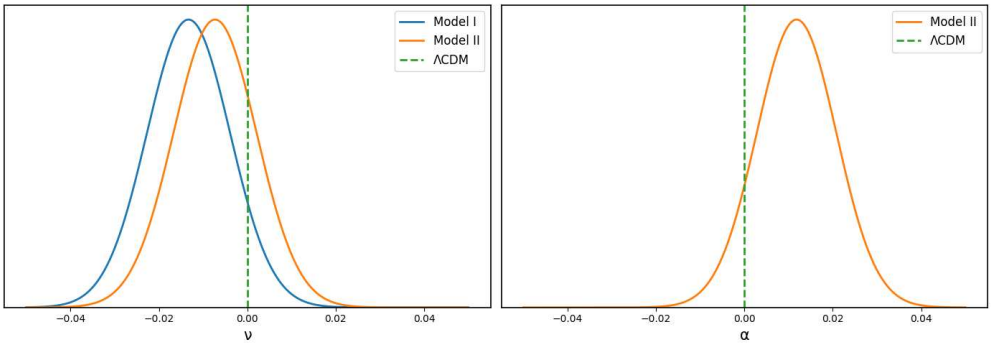

Figure 1. Posterior distributions of the RVE parameters ν and α. Model I is shown in blue and Model II in orange, both using the full dataset, while $\alpha = \nu = 0$ corresponds to the ΛCDM model (green dashed line).

Regarding Model II, as shown in Equation (34), this scenario introduces two additional RVE parameters relative to Model I, namely ν and α. In the limit $\nu, \alpha \to 0$, Model II reduces to the ΛCDM cosmology. For the Pantheon$^+$ + CC dataset, we obtain $(\nu, \alpha) = (-0.1510 \pm 0.0876,\ 0.3236 \pm 0.1464)$, corresponding to deviations from zero at the levels of 1.72σ and 2.21σ, respectively. Using the DESI BAO + CC combination, the constraints $(\nu, \alpha) = (0.0851 \pm 0.0786,\ 0.1363 \pm 0.0842)$ indicate milder deviations of 1.08σ and 1.62σ. For the CMB + CC data, we find $(\nu, \alpha) = (0.0431 \pm 0.0558,\ 0.0755 \pm 0.0494)$, corresponding to 0.77σ and 1.53σ deviations from zero, respectively. Using the full data, we obtain the mean values $\nu = -0.0073$, $\alpha = 0.0118$, and $\beta = 0.270$, which implies that the values of ν and α differ from zero at the level of 0.7σ and 1.3σ, respectively (see Figure 1). It is worth comparing our results with [83], where the authors also studied the second-order model, labeled as R2. In this case, taking into account $\alpha\dot{H}$ term with the condition $\alpha = -\nu$, they found $\nu = -0.532^{+0.024}_{-0.029}$ using SNIa + BAO + $H(z)$ measurements.

Figures 2 and 3 represent the 1D and 2D posterior distributions, representing the 68.3% (1σ) and 95.4% (2σ) confidence levels for the two RVE models, Models I and II, respectively. For Model I, Figure 2 shows positive correlations in (h, ω_b), (ν, ω_b), and (ν, Ω_m) planes, and negative correlations in (Ω_m, h) and (ν, h) planes. For Model II, Figure 3 illustrates positive correlations in (α, ν) and (β, Ω_m) planes, while (β, h) and (β, ν) planes exhibit negative correlations.

To evaluate and select the most appropriate model for explaining the DESI BAO + Pantheon$^+$ + CC + CMB datasets, which together comprise a total of $N_t = 1752$ observational data points. We employ three statistical criteria: AIC, BIC, and DIC, as shown in Table 3. In this analysis, the ΛCDM model is considered as the reference. For RVE-$f(Q)$ Model I, the AIC is nearly identical to that of ΛCDM ($\Delta\text{AIC}_{\text{Model I}} = -0.05$), while the DIC is slightly better ($\Delta\text{DIC}_{\text{Model I}} = -0.16$). This suggests an equivalent quality of fit compared to ΛCDM. However, BIC penalizes the inclusion of the additional parameter ν, yielding ($\Delta\text{BIC}_{\text{Model I}} = 2.46$).

For RVE-$f(Q)$ Model II, although the DIC remains nearly identical to the reference model ($\Delta\text{DIC}_{\text{Model II}} = 0.24$), the AIC difference increases to ($\Delta\text{AIC}_{\text{Model II}} = 2.46$), indicating only moderate support. Moreover, given the addition of three extra free parameters (ν, β, and α), the BIC rises significantly to ($\Delta\text{BIC}_{\text{Model II}} = 18.83$), clearly disfavoring this model because of its higher complexity. In summary, while ΛCDM remains the preferred model due to its simplicity, RVE-$f(Q)$ Model I emerges as the closest and most competitive alternative, challenging the standard cosmological model. In contrast, the complexity of RVE-$f(Q)$ Model II renders it much less favorable under the BIC criterion.

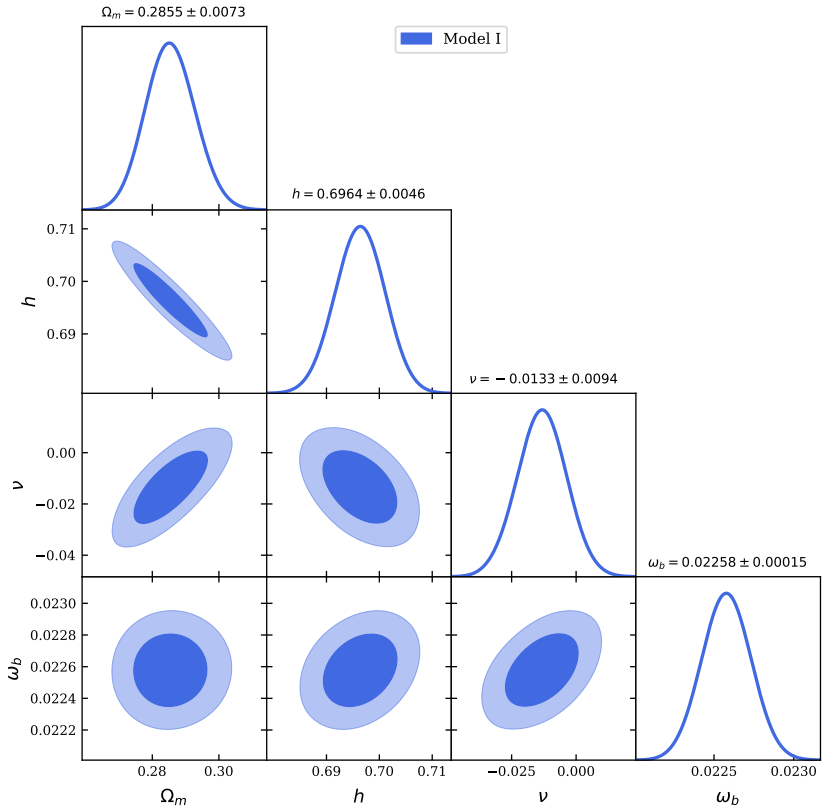

Figure 2. The 1σ and 2σ confidence contours and the posterior distributions obtained for the RVE-$f(Q)$ model I, using DESI BAO + Pantheon$^+$ + CC + CMB datasets.

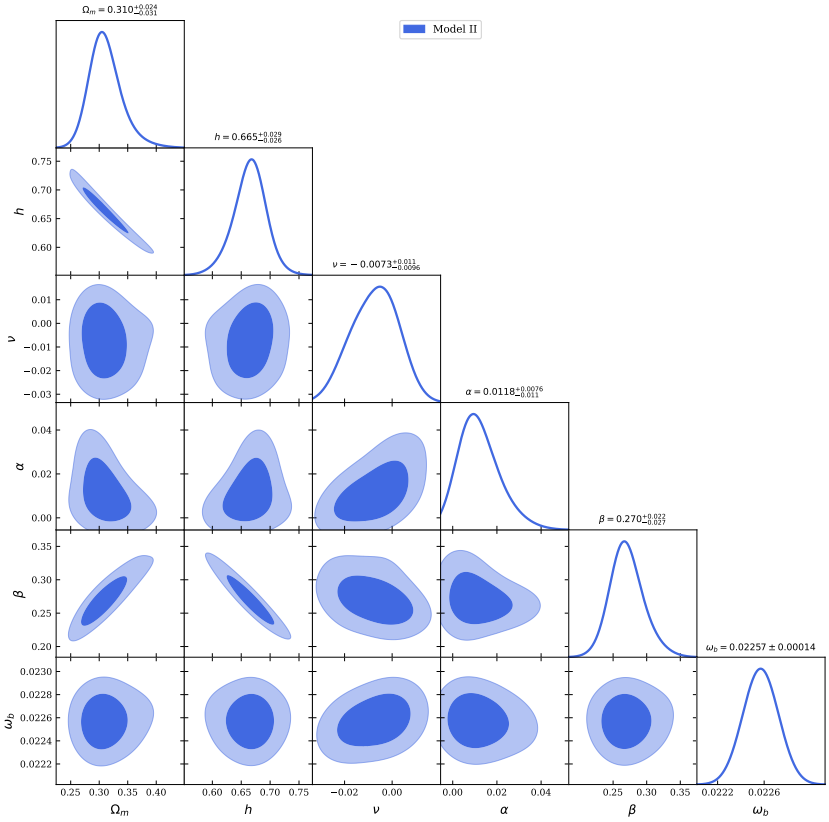

Figure 3. The 1σ and 2σ confidence contours and the posterior distributions obtained for the RVE-$f(Q)$ model II, using DESI BAO + Pantheon$^+$ + CC + CMB datasets.

At this stage, it is useful to compare our results with recent studies that have tested $f(Q)$ gravity using DESI data. In particular, the author in ref. [84] investigated a power-law model in $f(Q)$ gravity ($f(Q) \simeq Q^{\frac{n}{n-1}}$) within the non-coincident gauge and constrained it using DESI BAO data combined with Pantheon$^+$, gamma-ray bursts (GRB), and Observational Hubble Data (OHD). Although both analyses make use of DESI observations, the underlying theoretical frameworks and model parameterizations are different. In our case, the late-time cosmic acceleration is driven by a running vacuum energy component emerging directly from the modified Friedmann equations of $f(Q)$ gravity, without relying on an effective scalar-field description. Despite these differences, the inferred cosmological parameters show good agreement. For our most competitive scenario, namely the RVE-$f(Q)$ Model I, we obtain $h = 0.6964 \pm 0.0046$ and $\Omega_m = 0.2855 \pm 0.0073$ from the full dataset. These values are consistent with those reported in [84], with differences corresponding to 0.7σ in H_0 and 1.11σ in Ω_m when considering the SN + OHD + BAO + GRB dataset combination including DESI BAO data. This agreement indicates that DESI constraints on background cosmological parameters are robust across different realizations of $f(Q)$ gravity.

Figures 4–6 illustrate the cosmographic behavior of the ΛCDM model, Model I, and Model II using the full dataset combination (DESI BAO + Pantheon$^+$ + CC + CMB). Figure 4 shows the deceleration parameter as a function of redshift, defined as $q(t) = -\frac{1}{aH^2}\frac{d^2a}{dt^2}$. This quantity characterizes the acceleration state of the Universe: positive values of q correspond to a decelerating expansion, while negative values indicate accelerated expansion. All three models exhibit a transition from an early decelerating phase to a late-time accelerating phase. The transition redshift, defined by $q(z_t) = 0$, is found to be $z_t = 0.6893$, 0.7205, and 0.7717 for the ΛCDM model, Model I, and Model II, respectively. In contrast, Model II exhibits a positive value of the deceleration parameter at $z = 0$, which should not be interpreted as a physical decelerating Universe. This behavior originates from the analytic structure of the model and the presence of very small values of the parameter α. In particular, the term $(1+z)^{-3(1-\nu)/\alpha}$ becomes highly sensitive to small changes as $\alpha \to 0$, amplifying higher-order derivatives of the Hubble function. As a result, For Model II, the deceleration parameter becomes highly sensitive to the parameter α in the very low-redshift regime ($0 \lesssim z \lesssim 0.02$), leading to unphysical features in $q(z)$ near the present epoch, even though the model provides an excellent fit to the observational data.

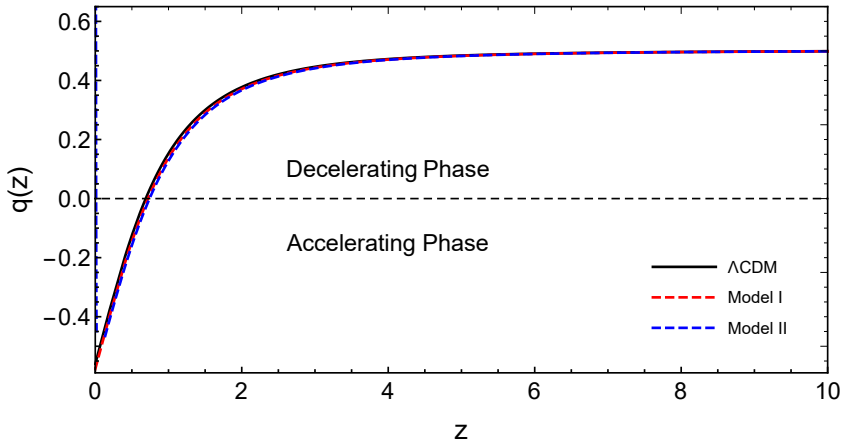

Figure 4. Deceleration parameter $q(z)$ as a function of the redshift z. The horizontal dashed line at $q = 0$ separates the decelerating ($q > 0$) and accelerating ($q < 0$) expansion phases. The solid black curve corresponds to the ΛCDM model, while the red dashed and blue dashed curves represent Model I and Model II, respectively.

Figure 5 presents the redshift evolution of the jerk parameter, defined as $j(t) = \frac{1}{aH^3}\frac{d^3a}{dt^3}$. In the ΛCDM scenario, the jerk parameter remains constant at $j = 1$ over the entire redshift

range, as expected. Model I closely follows this behavior, matching the ΛCDM prediction at the present epoch with $j_0 \simeq 1$, and exhibiting only a slow and smooth deviation from unity as the redshift increases. Model II displays a qualitatively similar evolution at intermediate and high redshifts, remaining very close to Model I for $z \gtrsim 0.05$. However, in the immediate vicinity of the present epoch, the jerk parameter of Model II exhibits a sharp, non-physical feature. This behavior originates from the strong sensitivity of third-order cosmographic derivatives to the small value of the parameter α, which amplifies higher-order derivatives of the Hubble function. Consequently, the cosmographic description of Model II becomes unreliable at very low redshift, while remaining well behaved at larger redshifts. Figure 6 shows the evolution of the snap parameter, $s(t) = \frac{1}{aH^4}\frac{d^4a}{dt^4}$, which probes even higher-order derivatives of the cosmic expansion. As expected, larger deviations from the ΛCDM behavior are observed for the extended models, particularly at low redshift. Model I exhibits a smooth and moderate departure from the ΛCDM prediction, whereas Model II shows a more pronounced deviation near the present epoch, again reflecting the enhanced sensitivity of higher-order cosmographic quantities to small values of α. Nevertheless, for $z \gtrsim 0.05$, the snap parameter in Model II converges toward a smooth behavior comparable to that of Model I.

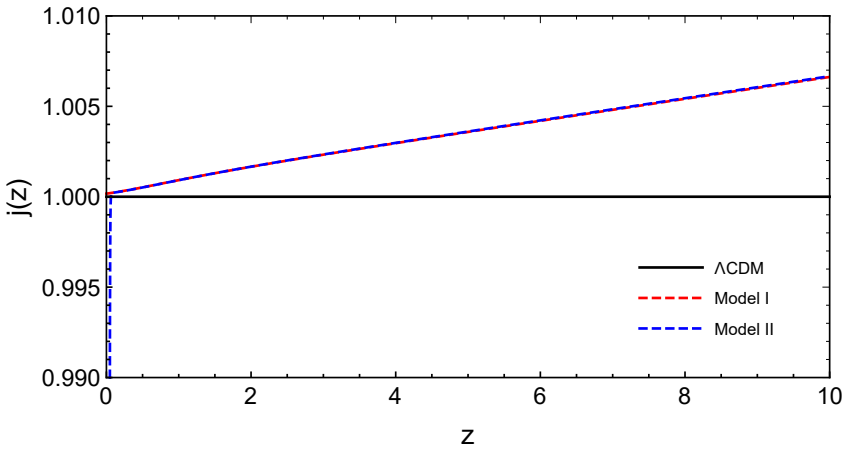

Figure 5. Jerk parameter $j(z)$ as a function of the redshift z. The horizontal black solid line at $j = 1$ corresponds to the ΛCDM model. The red dashed and blue dashed curves denote Model I and Model II, respectively.

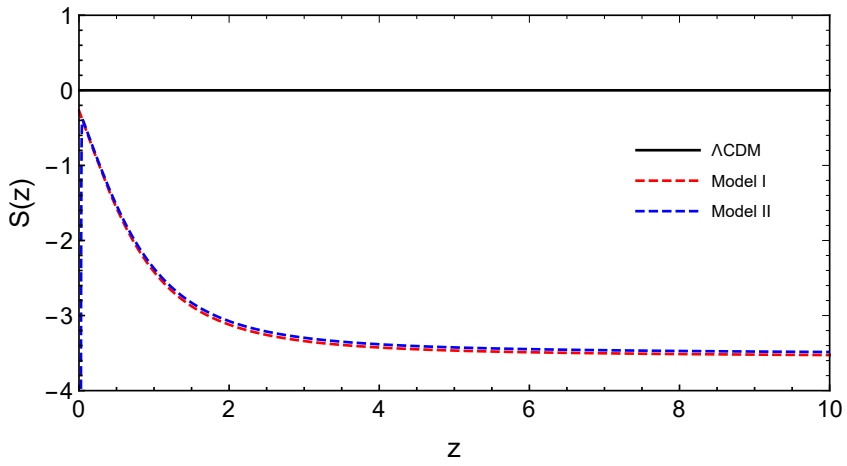

Figure 6. Snap parameter $s(z)$ as a function of the redshift z. The solid black curve corresponds to the ΛCDM model, while the red dashed and blue dashed curves represent Model I and Model II, respectively.

6. Conclusions

We have studied the running vacuum energy (RVE) within the framework of $f(Q)$ gravity, establishing a correspondence between the modified Friedmann equations of symmetric teleparallel gravity and the dynamical structure of vacuum energy. Following previous studies [23,50–52,68], we impose that the equation of state for RVE is not exactly equal to -1. A correction is therefore introduced such that $p_{\rm vac}(H) + \rho_{\rm vac}(H) = -\frac{\nu}{\kappa^2}\dot{H}$, meaning that the EoS receives a dynamical correction proportional to $\dot{H}$. To analyze this framework, we constructed two distinct scenarios: Model I, defined by $F_Q + 2QF_{QQ} = \text{const}$, and Model II, defined by $F_Q + 2QF_{QQ} = -\left(\nu + \frac{\alpha}{3}\frac{\ddot{H}}{H\dot{H}}\right)$, where the latter extends the framework to include a second-order involving $\ddot{H}/(H\dot{H})$.

Combining DESI BAO datasets with Pantheon$^+$ SNIa, cosmic chronometers, and CMB data, we performed a full MCMC analysis of the cosmological parameters. Both models yield fits consistent with current observations. Model I shows a mild ($\sim 1.4\sigma$) indication of a nonzero RVE parameter ν, while Model II exhibits weaker evidence, with ν and α constrained at the $\sim 0.7\sigma$ and 1.3σ levels, respectively. Model selection criteria further distinguish the scenarios: Model I is competitive with ΛCDM according to AIC and DIC, but BIC provides only moderate support due to the additional parameter ν. Model II is strongly penalized by the BIC, as well as by the sensitivity associated with the parameter α, rendering it less favored by the data.

In summary, establishing a correspondence between RVE and $f(Q)$ gravity offers a consistent and theoretically motivated extension of ΛCDM. Among the scenarios studied, Model I emerges as the most viable, providing a framework in which vacuum dynamics may contribute to alleviating the fine-tuning and coincidence problems, as well as the persistent H_0 tension. Ongoing and forthcoming high-precision data from DESI [74] and Euclid [85] will be decisive in testing these deviations.

Author Contributions: Conceptualization, D.M. and A.E.; methodology, D.M. and A.E.; software, D.M. and A.B.; validation, D.M., R.E.O., A.E. and A.B.; formal analysis, D.M.; investigation, D.M.; resources, D.M., R.E.O., A.E. and A.B.; data curation, D.M.; writing—original draft preparation, D.M., R.E.O. and A.E.; writing—review and editing, D.M., R.E.O., A.E. and A.B.; visualization, D.M.; supervision, A.E. and A.B.; project administration, A.E. and A.B.; funding acquisition, A.E. and A.B. All authors have read and agreed to the published version of the manuscript.

Funding: This research received no external funding.

Data Availability Statement: There are no new data associated with this article.

Conflicts of Interest: The authors declare no conflicts of interest.

Note

[1] ΔIC denotes ΔAIC, ΔBIC, and ΔDIC, defined as $\Delta IC = IC_{\rm model} - IC_{\rm ref}$.

References

1. Copel, E.J.; Sami, M.; Tsujikawa, S. Dynamics of dark energy. *Int. J. Mod. Phys. D* **2006**, *15*, 1753–1936. [CrossRef]
2. Weinberg, S. The Cosmological Constant Problem. *Rev. Mod. Phys.* **1989**, *61*, 1–23. [CrossRef]
3. Sahni, V.; Starobinsky, A.A. The Case for a positive cosmological Lambda term. *Int. J. Mod. Phys. D* **2000**, *9*, 373–444. [CrossRef]
4. Sivanandam, N. Is the Cosmological Coincidence a Problem? *Phys. Rev. D* **2013**, *87*, 083514. [CrossRef]
5. Velten, H.E.S.; vom Marttens, R.F.; Zimdahl, W. Aspects of the cosmological "coincidence problem". *Eur. Phys. J. C* **2014**, *74*, 1–8. [CrossRef]
6. Fujii, Y. Origin of the Gravitational Constant and Particle Masses in Scale Invariant Scalar—Tensor Theory. *Phys. Rev. D* **1982**, *26*, 2580. [CrossRef]
7. Ford, L.H. Cosmological constant damping by unstable scalar fields. *Phys. Rev. D* **1987**, *35*, 2339. [CrossRef]
8. Wetterich, C. Cosmology and the Fate of Dilatation Symmetry. *Nucl. Phys. B* **1988**, *302*, 668–696. [CrossRef]

9. Bouhmadi-Lopez, M.; Errahmani, A.; Martin-Moruno, P.; Ouali, T.; Tavakoli, Y. The little sibling of the big rip singularity. *Int. J. Mod. Phys. D* **2015**, *24*, 1550078. [CrossRef]
10. Bouali, A.; Albarran, I.; Bouhmadi-Lopez, M.; Errahmani, A.; Ouali, T. Cosmological constraints of interacting phantom dark energy models. *Phys. Dark Univ.* **2021**, *34*, 100907. [CrossRef]
11. Mhamdi, D.; Bargach, F.; Dahmani, S.; Bouali, A.; Ouali, T. Comparing phantom dark energy models with various diagnostic tools. *Gen. Rel. Grav.* **2023**, *55*, 11. [CrossRef]
12. Dahmani, S.; Bouali, A.; Bojaddaini, I.E.; Errahmani, A.; Ouali, T. Constraining neutrino properties and smoothing the Hubble tension via the LSBR model. *Gen. Rel. Grav.* **2023**, *55*, 22. [CrossRef]
13. Dahmani, S.; Bouali, A.; Bojaddaini, I.E.; Errahmani, A.; Ouali, T. Smoothing the H_0 tension with a phantom dynamical dark energy model. *Phys. Dark Univ.* **2023**, *42*, 101266. [CrossRef]
14. Chiba, T.; Okabe, T.; Yamaguchi, M. Kinetically driven quintessence. *Phys. Rev. D* **2000**, *62*, 23511. [CrossRef]
15. Malquarti, M.; Copeland, E.J.; Liddle, A.R.; Trodden, M. A New view of k-essence. *Phys. Rev. D* **2003**, *67*, 123503. [CrossRef]
16. Horava, P.; Minic, D. Probable values of the cosmological constant in a holographic theory. *Phys. Rev. Lett.* **2000**, *85*, 1610. [CrossRef]
17. Li, M. A Model of holographic dark energy. *Phys. Lett. B* **2004**, *603*, 1. [CrossRef]
18. Wang, S.; Wang, Y.; Li, M. Holographic dark energy. *Phys. Rept.* **2017**, *696*, 1. [CrossRef]
19. Belkacemi, M.H.; Bouhmadi-Lopez, M.; Errahmani, A.; Ouali, T. The holographic induced gravity model with a Ricci dark energy: Smoothing the little rip and big rip through Gauss-Bonnet effects? *Phys. Rev. D* **2012**, *85*, 83503. [CrossRef]
20. Bargach, F.; Bargach, A.; Bouhmadi-López, M.; Errahmani, A.; Ouali, T. A dynamical system approach to the holographic dark energy in a modified theory of gravity. *Int. J. Mod. Phys. D* **2021**, *30*, 2150076. [CrossRef]
21. Bouhmadi-Lopez, M.; Errahmani, A.; Ouali, T. The cosmology of an holographic induced gravity model with curvature effects. *Phys. Rev. D* **2011**, *84*, 083508. [CrossRef]
22. Gorini, V.; Kamenshchik, A.; Moschella, U. Can the Chaplygin gas be a plausible model for dark energy? *Phys. Rev. D* **2003**, *67*, 063509. [CrossRef]
23. Sola, J.; Gomez-Valent, A.; Perez, J.d. First evidence of running cosmic vacuum: Challenging the concordance model. *Astrophys. J.* **2017**, *836*, 43. [CrossRef]
24. Rezaei, M.; Malekjani, M.; Sola, J. Can dark energy be expressed as a power series of the Hubble parameter? *Phys. Rev. D* **2019**, *100*, 023539. [CrossRef]
25. George, P.; Shareef, V.M.; Mathew, T.K. Interacting holographic Ricci dark energy as running vacuum. *Int. J. Mod. Phys. D* **2018**, *28*, 1950060. [CrossRef]
26. Starobinsky, A.A. Disappearing cosmological constant in $f(R)$ gravity. *JETP Lett.* **2007**, *86*, 157–163. [CrossRef]
27. Sotiriou, T.P.; Faraoni, V. $f(R)$ Theories of Gravity. *Rev. Mod. Phys.* **2010**, *82*, 451–497. [CrossRef]
28. Sotiriou, T.P. 6+1 lessons from $f(R)$ gravity. *J. Phys. Conf. Ser.* **2009**, *189*, 12039. [CrossRef]
29. Cai, Y.F.; Capozziello, S.; Laurentis, M.D.; Saridakis, E.N. $f(T)$ teleparallel gravity and cosmology. *Rept. Prog. Phys.* **2016**, *79*, 106901. [CrossRef]
30. Bengochea, G.R.; Ferraro, R. Dark torsion as the cosmic speed-up. *Phys. Rev. D* **2009**, *79*, 124019. [CrossRef]
31. Capozziello, S.; Cardone, V.F.; Farajollahi, H.; Ravanpak, A. Cosmography in $f(T)$-gravity. *Phys. Rev. D* **2011**, *84*, 43527. [CrossRef]
32. Ouardi, R.E.; Bouali, A.; Bojaddaini, I.E.; Errahmani, A.; Ouali, T. Model-independent reconstruction of $f(T)$ gravity using genetic algorithms. *Chin. Phys.* **2025**, *49*, 115106. [CrossRef]
33. Jimenez, J.B.; Heisenberg, L.; Koivisto, T. Coincident General Relativity. *Phys. Rev. D* **2018**, *98*, 44048. [CrossRef]
34. Mhamdi, D.; Bouali, A.; Dahmani, S.; Errahmani, A.; Ouali, T. Cosmological constraints on $f(Q)$ gravity with redshift space distortion data. *Eur. Phys. J. C* **2024**, *84*, 310. [CrossRef]
35. Lazkoz, R.; Lobo, F.S.N.; Ortiz-Baños, M.; Salzano, V. Observational constraints of $f(Q)$ gravity. *Phys. Rev. D* **2019**, *100*, 104027. [CrossRef]
36. Mhamdi, D.; Bargach, F.; Dahmani, S.; Bouali, A.; Ouali, T. Constraints on Power Law and Exponential models in $f(Q)$ Gravity. *Phys. Lett. B* **2024**, *859* 139113. [CrossRef]
37. Sokoliuk, O.; Arora, S.; Praharaj, S.; Baransky, A.; Sahoo, P.K. On the impact of $f(Q)$ gravity on the large scale structure. *Mon. Not. Roy. Astron. Soc.* **2023**, *522*, 252–267. [CrossRef]
38. Enkhili, O.; Dahmani, S.; Mhamdi, D.; Ouali, T.; Errahmani, A. Cosmological constraints on a dynamical dark energy model in $f(Q)$ gravity. *Eur. Phys. J. C* **2024**, *84*, 806. [CrossRef]
39. Jimenez, J.B.; Heisenberg, L.; Koivisto, T.S.; Pekar, S. Cosmology in $f(Q)$ geometry. *Phys. Rev. D* **2020**, *101*, 103507. [CrossRef]
40. Mhamdi, D.; Dahmani, S.; Bouali, A.; Bojaddaini, I.E.; Ouali, T. Observational Constraints On the Growth Index Parameters in $f(Q)$ Gravity. *Fortschr. Phys.* **2025**, *73*, e70008. [CrossRef]
41. Capozziello, S.; D'Agostino, R. Model-independent reconstruction of $f(Q)$ non-metric gravity. *Phys. Lett. B* **2022**, *832*, 137229. [CrossRef]

42. Ouardi, R.E.; Bouali, A.; Dahmani, S.; Errahmani, A.; Ouali, T. Exploring $f(Q)$ gravity through model-independent reconstruction with genetic algorithms. *Phys. Lett. B* **2025**, *863*, 139374. [CrossRef]
43. Bouali, A.; Shukla, B.K.; Chaudhary, H.; Tiwari, R.K.; Samar, M.; Mustafa, G. Cosmological tests of parametrization q = $\alpha - \beta$ H in $f(Q)$ FLRW cosmology. *Int. J. Geom. Meth. Mod. Phys.* **2023**, *20*, 2350152. [CrossRef]
44. Harko, T. Thermodynamic interpretation of the generalized gravity models with geometry—Matter coupling. *Phys. Rev. D* **2014**, *90*, 44067. [CrossRef]
45. Errahmani, A.; Bouali, A.; Dahmani, S.; Bojaddaini, I.E.; Ouali, T. Constraining dark energy equations of state in $f(R,T)$ gravity. *Phys. Dark Univ.* **2024**, *45*, 101512. [CrossRef]
46. Moraes, P.H.R.S.; Sahoo, P.K. Modelling wormholes in $f(R,T)$ gravity. *Phys. Rev. D* **2017**, *96*, 44038. [CrossRef]
47. Xu, Y.; Li, G.; Harko, T.; Liang, S.D. Aspects of the cosmological "coincidence problem". *Eur. Phys. J. C* **2019**, *79*, 1–19.
48. Arora, S.; Pacif, S.K.J.; Bhattacharjee, S.; Sahoo, P.K. $f(Q,T)$ gravity models with observational constraints. *Phys. Dark Univ.* **2020**, *30*, 100664. [CrossRef]
49. Shekh, S.H.; Bouali, A.; Pradhan, A.; Beesham, A. J. New emergent observational constraints in f(Q,T) gravity model. *High Energy Astrophys.* **2023**, *39*, 53–69. [CrossRef]
50. Sola, J.; Gómez-Valent, A. The $\bar{\Lambda}$CDM cosmology: From inflation to dark energy through running Λ. *Int. J. Mod. Phys. D* **2015**, *24*, 1541003. [CrossRef]
51. Sola, J. The cosmological constant and entropy problems: Mysteries of the present with profound roots in the past. *Int. J. Mod. Phys. D* **2015**, *24*, 1544027. [CrossRef]
52. Moreno-Pulido, C.; Sola, J. Renormalizing the vacuum energy in cosmological spacetime: Implications for the cosmological constant problem. *Eur. Phys. J. C* **2022**, *82*, 551. [CrossRef]
53. Moreno-Pulido, C.; Sola, J.; Cheraghchi, S. Running vacuum in QFT in FLRW spacetime: The dynamics of $\rho_{\rm vac}(H)$ from the quantized matter fields. *Eur. Phys. J. C* **2023**, *83*, 637. [CrossRef]
54. Sola, J. The cosmological constant problem and running vacuum in the expanding universe. *Phil. Trans. Roy. Soc. A* **2022**, *380*, 20210182. [CrossRef]
55. Sola, J. Cosmological constant and vacuum energy: Old and new ideas. *J. Phys. Conf. Ser.* **2013**, *453*, 12015. [CrossRef]
56. Sola, J.; Gomez-Valent, A.; Perez, J.d.; Moreno-Pulido, C. Running vacuum against the H_0 and σ_8 tensions. *Europhys. Lett.* **2021**, *134*, 19001. [CrossRef]
57. Sola, J.; Gomez-Valent, A.; Perez, J.d.; Moreno-Pulido, C. Running Vacuum in the Universe: Phenomenological Status in Light of the Latest Observations, and Its Impact on the σ_8 and H_0 Tensions. *Universe* **2023**, *9*, 262. [CrossRef]
58. Basilakos, S.; Plionis, M.; Sola, J. Hubble expansion & Structure Formation in Time Varying Vacuum Models. *Phys. Rev. D* **2009**, *80*, 83511.
59. Gomez-Valent, A.; Sola, J. Vacuum models with a linear and a quadratic term in H: Structure formation and number counts analysis. *Mon. Not. R. Astron. Soc.* **2015**, *448*, 2810–2821. [CrossRef]
60. Geng, C.Q.; Lee, C.C.; Yin, L. Constraints on running vacuum model with $H(z)$ and $f\sigma_8$. *J. Cosmol. Astropart. Phys.* **2017**, *8*, 32. [CrossRef]
61. Sola, J. Dark energy: A Quantum fossil from the inflationary Universe? *J. Phys. A* **2008**, *41*, 164066. [CrossRef]
62. Padilla, L.E.; Tellez, L.O.; Escamilla, L.A.; Vazquez, J.A. Cosmological Parameter Inference with Bayesian Statistics. *Universe* **2021**, *7*, 213. [CrossRef]
63. Liddle, A.R. Information criteria for astrophysical model selection. *Mon. Not. Roy. Astron. Soc.* **2007**, *377*, L74–L78. [CrossRef]
64. Akaike, H. A new look at the statistical model identification. *IEEE Trans. Automat. Control* **1974**, *19*, 716–723. [CrossRef]
65. Schwarz, G. Estimating the Dimension of a Model. *Ann. Statist.* **1978**, *6*, 461–464. [CrossRef]
66. Spiegelhalter, D.J.; Best, N.G.; Carlin, B.P.; der Linde, A.V. Bayesian measures of model complexity and fit. *J. Roy. Stat. Soc. B* **2002**, *64*, 583–639. [CrossRef]
67. Moreno-Pulido, C.; Sola, J. Running vacuum in quantum field theory in curved spacetime: Renormalizing $\rho_{\rm vac}$ without m^4 terms. *Eur. Phys. J. C* **2020**, *80*, 1–23. [CrossRef]
68. Errahmani, A.; Magrach, M.; Dahmani, S.; Bouali, A.; Ouali, T. Emergence of running vacuum energy in $f(R,T)$ gravity: Observational constraints. *Phys. Lett. B* **2026**, *872*, 140040. [CrossRef]
69. Sola, J.; Moreno-Pulido, C.; Gonzalez-Fuentes, A. Running Vacuum and H^4 Inflation. *Universe* **2025**, *11*, 118. [CrossRef]
70. Gomez-Valent, A.; Sola, J.; Basilakos, S. Dynamical vacuum energy in the expanding Universe confronted with observations: A dedicated study. *J. Cosmol. Astropart. Phys.* **2015**, *1*, 4. [CrossRef]
71. Sola, J.; Gomez-Valent, A.; Perez, J.d. Hints of dynamical vacuum energy in the expanding universe. *Astrophys. J. Lett.* **2015**, *811*, L14. [CrossRef]
72. Lodha, K.; Shafieloo, A.; Calderon, R.; Linder, E.; Sohn, W.; Cervantes-Cota, J.L.; De Mattia, A.; García-Bellido, J.; Ishak, M.; Matthewson, W.; et al. DESI 2024: Constraints on physics-focused aspects of dark energy using DESI DR1 BAO data. *Phys. Rev. D* **2025**, *111*, 23532. [CrossRef]

73. Brieden, S.; Gil-Marín, H.; Verde, L. A tale of two (or more) h's. *J. Cosmol. Astropart. Phys.* **2023**, *4*, 23. [CrossRef]
74. Adame, A.G.; Aguilar, J.; Ahlen, S.; Alam, S.; Alexander, D.M.; Alvarez, M.; Alves, O.; Anand, A.; Andrade, U.; Armengaud, E.; et al. DESI 2024 VI: Cosmological constraints from the measurements of baryon acoustic oscillations. *J. Cosmol. Astropart. Phys.* **2025**, *2*, 21. [CrossRef]
75. Zhai, Z.; Wang, Y. Robust and model-independent cosmological constraints from distance measurements. *J. Cosmol. Astropart. Phys.* **2019**, *7*, 5. [CrossRef]
76. Brout, D.; Scolnic, D.; Popovic, B.; Riess, A.G.; Carr, A.; Zuntz, J.; Kessler, R.; Davis, T.M.; Hinton, S.; Jones, D.; et al. The Pantheon+ Analysis: Cosmological Constraints. *Astrophys. J.* **2022**, *938*, 2. [CrossRef]
77. Gaztanaga, E.; Cabre, A.; Hui, L. Clustering of luminous red galaxies–IV. Baryon acoustic peak in the line-of-sight direction and a direct measurement of $H(z)$. *Mon. Not. Roy. Astron. Soc.* **2009**, *399*, 1663. [CrossRef]
78. Lewis, A.; Bridle, S. Cosmological parameters from CMB and other data: A Monte Carlo approach. *Phys. Rev. D* **2002**, *66*, 103511. [CrossRef]
79. Gilks, W.R.; Richardson, S.; Spiegelhalter, D.J. *Markov Chain Monte Carlo in Practice*; Chapman and Hall/CRC: London, UK, 1995.
80. Mathew, T.K. Running vacuum model versus ΛCDM—A Bayesian analysis. *Mon. Not. Roy. Astron. Soc.* **2022**, *510*, 5553–5559.
81. Sola, J.; Perez, J.d.; Gomez-Valent, A. Possible signals of vacuum dynamics in the Universe. *Mon. Not. Roy. Astron. Soc.* **2018**, *478*, 4357–4373.
82. Tsiapi, P.; Basilakos, S. Testing dynamical vacuum models with CMB power spectrum from Planck. *Mon. Not. Roy. Astron. Soc.* **2019**, *485*, 2505. [CrossRef]
83. Rezaei, M.; Sola, J. Running vacuum versus holographic dark energy: A cosmographic comparison. *Eur. Phys. J. C* **2022**, *82*, 765. [CrossRef]
84. Paliathanasis, A. Testing non-coincident f(Q)-gravity with DESI DR2 BAO and GRBs. *Phys. Dark Univ.* **2025**, *49*, 101993. [CrossRef]
85. Mellier, Y.; Abdurroúf, A.; Barroso, J.A.; Achúcarro, A.; Adamek, J.; Adam, R.; Addison, G.E.; Aghanim, N.; Aguena, M.; Ajani, V.; et al. Euclid. I. Overview of the Euclid mission. *Astron. Astrophys.* **2025**, *697*, A1.